doi:10.1093/brain/awz125 BRAIN 2019: 142; 1955–1972 | 1955

BRAIN
A JOURNAL OF NEUROLOGY

Characterizing the role of the structural connectome in seizure dynamics

Preya Shah,[1,2] Arian Ashourvan,[1,2] Fadi Mikhail,[2,3] Adam Pines,[4] Lohith Kini,[1,2] Kelly Oechsel,[2,3] Sandhitsu R. Das,[3] Joel M. Stein,[5] Russell T. Shinohara,[6] Danielle S. Bassett,[1,2,3,7,8] Brian Litt[1,2,3] and Kathryn A. Davis[2,3]

How does the human brain's structural scaffold give rise to its intricate functional dynamics? This is a central question in translational neuroscience that is particularly relevant to epilepsy, a disorder affecting over 50 million subjects worldwide. Treatment for medication-resistant focal epilepsy is often structural—through surgery or laser ablation—but structural targets, particularly in patients without clear lesions, are largely based on functional mapping via intracranial EEG. Unfortunately, the relationship between structural and functional connectivity in the seizing brain is poorly understood. In this study, we quantify structure-function coupling, specifically between white matter connections and intracranial EEG, across pre-ictal and ictal periods in 45 seizures from nine patients with unilateral drug-resistant focal epilepsy. We use high angular resolution diffusion imaging (HARDI) tractography to construct structural connectivity networks and correlate these networks with time-varying broadband and frequency-specific functional networks derived from coregistered intracranial EEG. Across all frequency bands, we find significant increases in structure-function coupling from pre-ictal to ictal periods. We demonstrate that short-range structural connections are primarily responsible for this increase in coupling. Finally, we find that spatiotemporal patterns of structure-function coupling are highly stereotyped for each patient. These results suggest that seizures harness the underlying structural connectome as they propagate. Mapping the relationship between structural and functional connectivity in epilepsy may inform new therapies to halt seizure spread, and pave the way for targeted patient-specific interventions.

1 Department of Bioengineering, School of Engineering and Applied Science, University of Pennsylvania, Philadelphia, PA, 19104, USA
2 Center for Neuroengineering and Therapeutics, University of Pennsylvania, Philadelphia, PA, 19104, USA
3 Department of Neurology, Perelman School of Medicine, University of Pennsylvania, Philadelphia, PA, 19104, USA
4 Department of Neuroscience, Perelman School of Medicine, University of Pennsylvania, Philadelphia, PA, 19104, USA
5 Department of Radiology, Perelman School of Medicine, University of Pennsylvania, Philadelphia, PA, 19104, USA
6 Department of Biostatistics, Epidemiology, and Informatics, Perelman School of Medicine, University of Pennsylvania, Philadelphia, PA, 19104, USA
7 Department of Electrical and Systems Engineering, School of Engineering & Applied Science, University of Pennsylvania, Philadelphia, PA, 19104, USA
8 Department of Physics and Astronomy, College of Arts and Sciences, University of Pennsylvania, Philadelphia, PA, 19104, USA

Correspondence to: Preya Shah
Department of Bioengineering, School of Engineering and Applied Science, University of Pennsylvania, Philadelphia, PA, 19104, USA
E-mail: preya@pennmedicine.upenn.edu

Keywords: epilepsy; intracranial EEG; high-angular resolution diffusion imaging; structural connectivity; functional connectivity

Abbreviations: DTI = diffusion tensor imaging; DWI = diffusion-weighted imaging; HARDI = high angular resolution diffusion imaging; iEEG = intracranial EEG; MEG = magnetoencephalography; SC-FC = structural-functional connectivity

Received September 4, 2018. Revised February 11, 2019. Accepted March 7, 2019. Advance Access publication May 17, 2019

Introduction

Epilepsy is a neurological disorder characterized by recurrent, unprovoked seizures. It affects over 50 million subjects worldwide (World Health Organization, 2018) and will afflict ~1 in 26 subjects during their lifetime (Hesdorffer *et al.*, 2011). The most common subtype is focal or localization-related epilepsy, in which seizures arise from a specific region in the brain (French, 2007). Patients with localization-related epilepsy often experience uncontrolled seizures despite medication, leading to neurological and psychiatric co-morbidities, deterioration in quality of life, and up to an 11-fold increase in mortality rate (Kwan *et al.*, 2011; Fazel *et al.*, 2013).

Structural brain lesions are considered to be at the core of the epileptogenic zone in localization-related epilepsy (Bernasconi, 2017). Indeed, targeted surgical removal of contiguous regions of abnormal brain tissue has high seizure-freedom rates in drug-resistant epilepsy patients, up to 80% (Spencer *et al.*, 2005; De Tisi *et al.*, 2011; Hussan *et al.*, 2012; Wiebe, 2012; Jette and Wiebe, 2013). However, seizures also may involve recruitment of and spread to multiple, often distant brain regions, thereby involving distributed brain networks (Kramer and Cash, 2012; Bernhardt *et al.*, 2013). As a result, researchers are applying graph theoretical methods from the rapidly growing field of network neuroscience to identify brain network abnormalities in epilepsy, in the hope of finding targets for therapeutic interventions. In this approach, investigators map whole-brain structural and functional networks, or 'connectomes', by characterizing connectivity between brain regions based on multi-modal neuroimaging data (Bullmore and Sporns, 2009; Rubinov and Sporns, 2010; Bassett and Sporns, 2017). Structural brain networks are most commonly derived from diffusion tensor imaging (DTI) tractography (Hagmann *et al.*, 2008). Functional brain networks are most commonly derived from correlations in signal fluctuations across multiple recording sites from modalities such as resting state functional MRI (Biswal *et al.*, 1995; Salvador *et al.*, 2004), magnetoencephalography (MEG) (Stam, 2004), and EEG (Micheloyannis *et al.*, 2006). These approaches reveal a wide variety of network disruptions in epilepsy patients, both structurally (Raj *et al.*, 2010; Vaessen *et al.*, 2012; Taylor *et al.*, 2015) and functionally (Pittau *et al.*, 2012; Pedersen *et al.*, 2015; de Campos *et al.*, 2016; Shah *et al.*, 2019). While still nascent, this work shows promise for clinical applications, as network-based measures may serve as biomarkers for predicting seizure onset and spread (Burns *et al.*, 2014; Khambhati *et al.*, 2016; Jirsa *et al.*, 2017; Proix *et al.*, 2017), cognitive impairments (Vlooswijk *et al.*, 2011; Vaessen *et al.*, 2012), and outcome following surgical therapy (Goodfellow *et al.*, 2016; Sinha *et al.*, 2017; Lopes *et al.*, 2018).

Most studies of epileptic networks focus solely on either structural or functional connectivity. However, it is commonly understood that the two are tightly linked. In fact, there is great interest in the neuroscience community in elucidating the relationship between brain structure and function. Recent evidence shows that structural and functional brain networks are correlated at multiple temporal and spatial scales, that structural connectivity constrains functional connectivity, and that functional connectivity can modulate structural connectivity via mechanisms of plasticity (Skudlarski *et al.*, 2008; Greicius *et al.*, 2009; Honey *et al.*, 2009; Rubinov *et al.*, 2009; van den Heuvel *et al.*, 2009; Zhang *et al.*, 2010; Hagmann *et al.*, 2010; Hermundstad *et al.*, 2013, 2014; Chu *et al.*, 2015; Finger *et al.*, 2016).

Given the robust coupling between structure and function in healthy brains, disruptions in structure-function coupling can serve as biomarkers of neurological disease, including epilepsy. For example, Zhang *et al.* (2011) report that the degree of coupling between resting-state functional MRI networks and DTI tractography networks is lower in idiopathic generalized epilepsy patients compared with healthy controls, and is negatively correlated with epilepsy duration. Using a similar approach, Chiang *et al.* (2015) report decreased structure-function coupling in patients with left temporal lobe epilepsy compared with healthy subjects. These two studies use resting-state functional MRI, which characterizes the static, interictal functional epileptic network. However, little is known about the correlation between structural and functional connectivity during seizures. How does structure-function coupling change over the course of seizure evolution? And which particular connections drive these changes? Clinically, it is well understood that focal seizures often quickly spread to distant brain regions, but the relationship of this spread to underlying structure has not been quantified. Understanding where seizures are generated and how they spread has been hampered by sparsely sampled intracranial EEG and lesion-negative clinical brain images, and yet remains vital for planning surgical treatments for epilepsy.

To address these questions, we studied structure-function coupling in 45 seizures from nine drug-resistant localization-related epilepsy patients undergoing routine evaluation for epilepsy surgery. To construct time-varying functional connectivity (FC) networks, we used clinical recordings from intracranial EEG (iEEG), an invasive method that captures electrical activity from the brain in the form of aggregate local field potentials, at high spatial and temporal resolution (Penfield and Jasper, 1954). To construct structural connectivity (SC) networks, we used high angular resolution diffusion imaging (HARDI), an advanced diffusion imaging method that can produce robust tractography results in regions of crossing white matter pathways (Tuch *et al.*, 2002). We characterized relationships between these two modalities across time, frequency, and space. We hypothesized that there would be an increase in structure-function coupling during the progression from pre-ictal to ictal states, as seizures spread along structural pathways. Our findings shed light on the pathophysiological processes involved in seizure dynamics, which can ultimately inform

new approaches for clinical intervention. We detail these investigations below.

Materials and methods

Subjects

We studied nine patients undergoing pre-surgical evaluation for drug-resistant epilepsy at the Hospital of the University of Pennsylvania. Inclusion criteria for these patients consisted of all patients who agreed to participate in our research scanning protocol and allowed their de-identified iEEG data to be publicly available for research purposes on the International Epilepsy Electrophysiology Portal (www.ieeg.org, IEEG Portal) (Wagenaar *et al.*, 2013; Kini *et al.*, 2016). Seizure localization was determined via comprehensive clinical evaluation, which included multimodal imaging, scalp and intracranial video-EEG monitoring, and neuropsychological testing. This study was approved by the Institutional Review Board of the University of Pennsylvania, and all subjects provided written informed consent prior to participating.

Intracranial EEG acquisition

Cortical surface and depth electrodes were implanted in patients based on clinical necessity. Electrode configurations (Ad Tech Medical Instruments) consisted of linear cortical strips and two-dimensional cortical grid arrays (2.3 mm diameter with 10 mm inter-contact spacing) and linear depths (1.1 mm diameter with 10 mm inter-contact spacing). Continuous iEEG signals were obtained for the duration of each patient's stay in the epilepsy monitoring unit. Signals were recorded at 500 Hz. For each clinically identified seizure event, a board-certified epileptologist precisely annotated the onset time, termination time, seizure type, and electrodes recording artefact signals. Seizure onset times were defined by the earliest electrographic change (Litt *et al.*, 2001). Seizure types were classified using ILAE 2017 criteria (Fisher *et al.*, 2017) as focal aware (previously known as simple partial), focal impaired awareness (previously known as complex partial), or focal to bilateral tonic-clonic (previously known as complex partial with secondary generalization). Furthermore, the onset time of bilateral spread was noted for focal to bilateral tonic-clonic seizures. All annotations were verified and consistent with detailed clinical documentation. To ensure consistency and validity of the captured seizures, we discarded seizures that contained substantial artefacts in all electrodes, events that were short (<15 s), or those that occurred during sleep.

Image acquisition

Prior to electrode implantation, MRI data were collected on a 3 T Siemens Magnetom Trio scanner using a 32-channel phased-array head coil. High-resolution anatomical images were acquired using a magnetization prepared rapid gradient-echo (MPRAGE) T_1-weighted sequence (repetition time = 1810 ms, echo time = 3.51 ms, flip angle = 9°, field of view = 240 mm, resolution = $0.94 \times 0.94 \times 1.0$ mm^3). HARDI was acquired with a single-shot EPI multi-shell diffusion-weighted imaging (DWI) sequence (116 diffusion sampling directions, *b*-values of 0, 300, 700 and 2000 s/mm^2, resolution = $2.5 \times 2.5 \times 2.5$ mm^3 resolution, field of view = 240 mm). The same HARDI sequence was acquired in nine healthy adult control subjects for the purpose of comparison. Following electrode implantation, spiral CT images (Siemens) were obtained clinically for the purposes of electrode localization. Both bone and tissue windows were obtained (120 kV, 300 mA, axial slice thickness = 1.0 mm).

Region of interest selection

A brain network consists of nodes representing regions of interest within the brain, and edges representing the strength of connectivity between these regions of interest. To carry out direct quantitative comparisons of structural and functional networks, it was necessary to establish a direct correspondence between functional network nodes and structural network nodes. We therefore determined the location of each electrode in Montreal Neurological Institute (MNI) space and assigned each electrode to its nearest structural region of interest.

Structural regions of interest were defined by an upsampled version of the Automated Anatomical Labeling Atlas (Tzourio-Mazoyer *et al.*, 2002), which consisted of 600 roughly equally sized (region of interest sizes averaging 2.14 ± 0.28 cm^3) anatomically constrained regions covering the entire brain with the exception of the cerebellum. We chose this atlas (AAL-600) because it has regions of interest of the same order of resolution as iEEG, obeys gross anatomical boundaries, and has successfully been used in prior studies to evaluate structural and functional connectivity patterns in the brain (Hermundstad *et al.*, 2013, 2014).

To determine electrode MNI coordinates, electrodes were first identified via thresholding of the CT image and labelled using a semi-automated process. Each patient's CT and T_1-weighted MRI images were aligned using 3D rigid affine registration, with mutual information as the similarity metric. The T_1-weighted MRI images were then aligned to the standard MNI brain using diffeomorphic registration with the symmetric normalization (SyN) method (Avants *et al.*, 2008). The resulting transformations were used to warp the coordinates of the electrode centroids into MNI space. Co-registrations and transformations were carried out using Advanced Normalization Tools (ANTS) software (Avants *et al.*, 2009, 2011), and the accuracy of each step was confirmed via visual inspection. In our final framework, electrodes served as nodes of the functional networks and the associated structural regions of interest served as nodes of the structural networks.

Structural network generation

Diffusion-weighted images were skull-stripped via the FSL brain extraction tool and underwent eddy current and motion correction via the FSL eddy tool (Andersson and Sotiropoulos, 2016). Next, DWI susceptibility distortions were mitigated using the structural T_1-weighted image as follows: (i) T_1-weighted images were registered to the b0 image from the DWI scans using FSL FLIRT boundary-based registration (Greve and Fischl, 2009); (ii) T_1-weighted images were contrast inverted and intensity matched to the DWI image; and (iii) the DWI scans underwent non-linear

transformation to the T_1-weighted scan (Wang *et al.*, 2017). Following these preprocessing steps, DSI-Studio (http://dsi-studio.labsolver.org) was used to reconstruct the orientation density functions within each voxel using generalized q-sample imaging with a diffusion sampling length ratio of 1.25 (Yeh *et al.*, 2010). Deterministic whole-brain fibre tracking was performed using an angular threshold of 35 degrees, step size of 1 mm, and quantitative anisotropy threshold based on Otsu's threshold (Otsu, 1979). Tracks with length shorter than 10 mm or longer than 400 mm were discarded, and a total of 1 000 000 tracts were generated per brain. Deterministic tractography was chosen based upon prior work indicating that deterministic tractography generates fewer false positive connections than probabilistic approaches, and that network-based estimations are substantially less accurate when false positives are introduced into the network compared with false negatives (Zalesky *et al.*, 2010).

Subject-level AAL-600 atlases were generated in DWI space by applying the previously generated registration transformations from MNI to T_1-weighted space and from T_1-weighted space to DWI space. Finally, structural networks were generated by computing the number of streamlines connecting each pair of structural regions of interest identified above. The distribution of mean streamline lengths between each pair of structural regions of interest for each patient is illustrated in Supplementary Fig. 1. As the structural regions of interest were selected based on presence of electrodes, the range and distributions of mean streamline lengths were inherently highly dependent on the number and anatomical locations of electrodes. Streamline counts were subsequently log-transformed to improve normality of the distribution, as is common in prior studies (Bonilha *et al.*, 2015; Wirsich *et al.*, 2016; Park *et al.*, 2017; Taylor *et al.*, 2018).

Functional network generation

Each seizure event consisted of an ictal period spanning the time between seizure onset (earliest electrographic change) and termination, and an associated pre-ictal period of equivalent duration immediately prior to seizure onset. For the purpose of subsequent analyses, for each ictal period we also selected a corresponding interictal period of equivalent duration at least 6 h away from seizure activity, and a 5 min postictal period immediately following seizure termination. Following removal of artefact-ridden electrodes, intracranial EEG signals for each period were common-average referenced to reduce potential sources of correlated noise (Ludwig *et al.*, 2009). Next, each period was divided into 1 s non-overlapping time windows in accordance with previous studies (Kramer *et al.*, 2010; Khambhati *et al.*, 2015, 2016, 2017).

To generate a functional network representing broadband functional interactions between iEEG signals for each 1-s time window, we carried out a method described in detail previously (Khambhati *et al.*, 2017). Namely, signals were notch-filtered at 60 Hz to remove power line noise, low-pass and high-pass filtered at 115 Hz and 5 Hz to account for noise and drift, and pre-whitened using a first-order autoregressive model to account for slow dynamics. Functional networks were then generated by applying a normalized cross-correlation function ρ between the signals of each pair of electrodes within each time window, using the formula:

$$\rho_{xy}(k) = \underset{\tau}{argmax}\left[\frac{1}{T}\sum_{t}\frac{(x_k(t)-\bar{x}_k)(y_k(t+\tau)-\bar{y}_k)}{\sigma_{x_k}\sigma_{y_k}}\right] \quad (1)$$

where x and y are signals from two electrodes, k is the 1 s time window, t is one of the T samples during the time window, and τ is the time lag between signals, with a maximum lag of 250 ms. Next, to gain an understanding of the frequency dependence of structural–functional connectivity (SC-FC) relationships, we generated functional networks across physiologically relevant frequency bands as described in detail in a previous study (Khambhati *et al.*, 2016). Specifically, multitaper coherence estimation (time-bandwidth product of 5, 8 tapers) was used to compute functional coherence networks for each 1 s window across four frequency bands: α/θ (5–15 Hz), β (15–25 Hz), low-γ (30–40 Hz), and high-γ (95–105 Hz). Both broadband and frequency-specific networks were represented as full-weighted adjacency matrices for each 1-s window in each period.

Structure-function coupling analysis

To quantify the relationship between structure and function in the epileptic brain, we computed the Pearson correlation coefficient between the edges of each structural connectivity network and the edges of each broadband functional connectivity network, followed by Fisher *r-z* transformation for variance stabilization (Fisher, 1921). This led to a time series of SC-FC correlations for each seizure event in each subject. To understand the frequency-dependence of SC-FC coupling better, we repeated the same analysis using the frequency-specific functional networks.

Next, to understand the extent to which the resulting SC-FC time series evolve similarly within each subject, we computed the Euclidean distances between these time series for all pairs of seizure events. Importantly, we first time-normalized the time series for each seizure event to span 200 evenly spaced time bins (100 pre-ictal and 100 ictal). Next, for each seizure event, we generated a single vector consisting of the SC-FC time series for all five frequency bands: broadband, α/θ, β, low-γ, and high-γ. Euclidean distances were then computed between all pairs of vectors, composed of pairs belonging to the same patient and pairs belonging to different patients.

Finally, we wished to assess which edges in the structural network were responsible for the changes in SC-FC correlation between pre-ictal and ictal periods. We therefore first computed a mean ictal and mean pre-ictal broadband functional network for each subject by averaging across seizures events and across windows within each time period. Next, we carried out a virtual edge resection approach, in which we removed an edge from the network and computed the change in SC-FC correlation, $\Delta z(i)$, as follows:

$$\Delta z(i) = N[z - z^i] \quad (2)$$

where z is the SC-FC correlation, z^i is the SC-FC correlation following removal of edge i, and N is the number of edges in the network. We chose to multiply by N to normalize the scale of Δz across subjects with different numbers of edges. We performed this calculation for both pre-ictal and ictal

time periods. Since we were specifically interested in edges that statistically contribute to the increase in SC-FC correlation during seizures, we defined a measure of *contribution*, $\sigma(i)$, for each edge i in which a structural connection exists on the increase in SC-FC correlation during seizures as follows:

$$\sigma(i) = [\Delta z_{ictal}(i) - \Delta z_{pre\text{-}ictal}(i)] \quad (3)$$

where $\Delta z_{ictal}(i)$ and $\Delta z_{pre\text{-}ictal}(i)$ are the relative changes in SC-FC correlations following removal of edge i during the ictal and pre-ictal periods, respectively.

We defined 'contributors' of SC-FC correlation during seizures as structural edges with $\Delta z_{ictal}(i) > 0$ and $\sigma(i) > 0$. This is because we wanted to identify regions that positively contributed to SC-FC correlation ictally, and more so ictally than pre-ictally. To understand the properties of contributor edges better, we computed the lengths of both the contributor edges and non-contributor edges, in terms of both streamline length and Euclidean distance. The purpose of this analysis was to determine whether the increased SC-FC correlation during seizures was due to long- or short-range connections. The Euclidean distance of an edge was calculated using the mean voxel coordinates of two regions of interest connected by that edge. The streamline length of an edge was calculated using the mean length of all tracts between the pair of regions of interest connected by that edge. To understand the relationship between structure-function coupling and functional seizure spread, for each structurally connected edge i we computed the correlation between contribution and the change in function edge weight between ictal and pre-ictal periods.

A summary of our patient-level SC-FC analysis pipeline is illustrated in Fig. 1.

Characterization of structural properties in relation to structure-function changes

We wanted to probe whether there were any factors in patients' brain structure, both in terms of global structural connectivity and local microstructure, which might account for the observed structure-function coupling dynamics. First, to determine whether global structural network topology was significantly different in patients compared to healthy controls, we generated structural networks as described above in nine healthy adult subjects. Next, in both groups, we computed and compared global clustering coefficient, global efficiency, and small-worldness, network properties that have proven particularly useful in characterizing brain graph topology and quantify the brain's capacity to minimize biological while maximizing topological integration (Bullmore and Sporns, 2009; Bassett and Bullmore, 2017) (see Supplementary material for equations and further details).

Next, to determine whether seizure spread is affected by local structure in addition to structural connectivity, we computed DTI-derived microstructural indices for each structural region of interest and correlated them with the degree of ictal versus pre-ictal changes in functional connectivity and structure-function coupling. Specifically, we computed fractional anisotropy (FA) and mean diffusivity (MD), the two most commonly studied DTI metrics which quantify the magnitude and preferred directionality of water diffusion within each voxel. For each region of interest, we then computed the mean SC-FC contribution of that region of interest by averaging the contributions of all edges emanating from that region of interest. Similarly, we computed the mean change

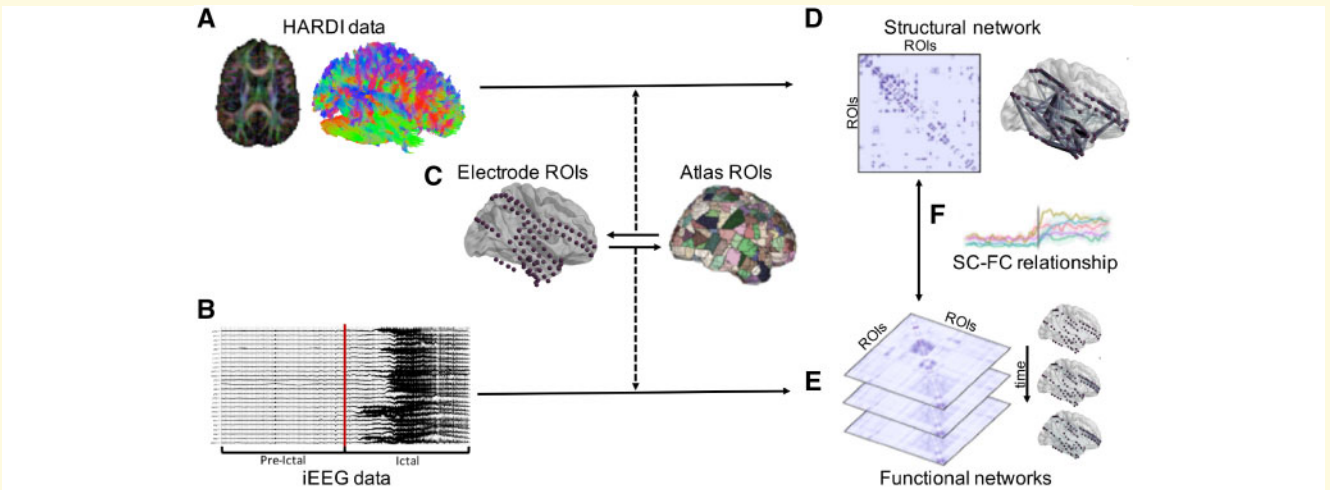

Figure 1 Summary of patient-level SC-FC analysis pipeline. (**A**) HARDI preprocessing and whole-brain tractography was carried out. (**B**) iEEG data were preprocessed and seizures were annotated, with each seizure event consisting of an ictal period and an associated pre-ictal period of equivalent duration. (**C**) Regions of interest (ROIs) were selected via a one-to-one spatial correspondence between electrode centroids and atlas regions. (**D**) The structural connectivity (SC) network was generated using log-normalized streamline counts between atlas regions of interest associated with each electrode location. (**E**) Time-varying broadband functional connectivity (FC) networks were generated for each 1 s time window by computing correlation between iEEG signals across electrode pairs. Frequency-specific functional connectivity networks were similarly computed using coherence between iEEG signals across electrode pairs. (**F**) SC-FC relationships were quantified across time, frequency, and space (see 'Materials and methods' section for details).

in functional connectivity between ictal and pre-ictal periods for each region of interest. For each patient, we then correlated the mean value of each microstructural measure with both the mean contribution and mean functional connectivity change, across regions of interest.

Statistical analyses

To determine whether the SC-FC correlations were significantly greater than chance, for each 1-s window we generated a null distribution of correlations via random permutation of the functional network edges (10 000 permutations). We then compared the mean SC-FC correlations during ictal and pre-ictal periods with the null correlations. Next, to determine whether there was a significant increase in SC-FC correlation between pre-ictal and ictal periods, we computed the difference between the mean ictal z and the mean pre-ictal z for each seizure event. We modelled these paired differences using a linear mixed effects model with subject assignment as the random effect, and determined whether the difference was significantly greater than zero using the parametric bootstrap method (1000 bootstrapped samples), which is robust to small sample sizes (Davison and Hinkley, 1997; Halekoh and Højsgaard, 2014). To assess whether the findings were robust to our choice of non-ictal period, we repeated the above analysis substituting the pre-ictal periods with interictal periods of equivalent duration that were at least 6 h away from seizure activity. To further compare findings during pre-ictal and interictal periods, we also carried out the above statistical analysis to determine significant differences between mean pre-ictal z and mean interictal z. Finally, to better understand the pattern of SC-FC coupling during the early post-ictal period, we also carried out the above statistical analysis to determine significant differences between mean ictal z and mean postictal z. The 5 min postictal period was divided into two subperiods: one consisting of the first 1 min following seizure termination, and one consisting of the subsequent 4 min.

To assess the degree of intra-subject similarity of SC-FC evolution across the pre-ictal and ictal periods, we compared the between-subject time series Euclidean distances to the within-subject time series Euclidean distances and tested the significance of the difference using permutational multivariate ANOVA (PERMANOVA) (999 permutations) (Anderson, 2017).

To characterize the properties of edges that contribute to the increase in SC-FC correlation during seizures, we computed the mean length of all contributor edges and the mean length of all non-contributor edges for each subject. Edge length was computed using two metrics: mean streamline length, and Euclidean distance. We compared the mean contributor and non-contributor edge lengths using a paired t-test. Furthermore, to assess the relationship between edge contribution and edge length among the contributor edges, we classified contributor edges into 'low', 'medium', and 'high' contribution levels for each subject using tertiles. The edge lengths in these three categories were compared using paired t-tests. Finally, given prior knowledge that structural connection weights decrease with Euclidean distance (Kaiser and Hilgetag, 2004; Lewis *et al.*, 2009; Rubinov *et al.*, 2015; Donahue *et al.*, 2016), we repeated all analyses after removing the effect of Euclidean distance from the structural networks using linear regression. More specifically, we fit a generalized linear model with the vector of all structural edges as the dependent variable and the vector of Euclidean distances as the independent variable, and took the residuals. The residuals were used for the repeat analysis. Given that this study takes a connectivity-based approach (i.e. focusing on connections/edges between regions of interest rather than the regions of interest themselves), this regression approach accounts for the distance-dependent effects of both the connection weights and the number of different structural connections. This is because each region of interest is associated with a number of different structural connections (i.e. edges), and each edge is associated with a different weight.

Data availability

De-identified iEEG recordings are available online on the International Epilepsy Electrophysiology Portal (www.ieeg.org, IEEG Portal). Our network analysis scripts and associated visualizations are publicly available at https://github.com/shah-preya/EpiConn.

Results

Clinical data

Forty-five clinical seizures (mean duration 71 s ± 44 s), were recorded across the nine patients (mean age 40.2 ± 11.8; five female). All seizures had focal onset, and were characterized as focal aware, focal impaired awareness, or focal to bilateral tonic-clonic. Patient demographic and clinical details, along with final number of regions of interest, are detailed in Table 1.

SC-FC coupling using broadband functional connectivity

To assess the overall temporal patterns of SC-FC coupling changes during seizures, we first quantified SC-FC correlations using broadband functional connectivity networks. For each individual seizure event, we determined the degree of SC-FC coupling, as measured by the Fisher-transformed Pearson correlation, z (Fig. 2A). For all seizures in all subjects, SC-FC coupling was significantly greater than chance during interictal, pre-ictal and ictal periods ($P < 0.05$, permutation-based testing; Fig. 2B). While the temporal progression of SC-FC changes was subject-specific (Fig. 2C), there was a consistent increase between pre-ictal and ictal periods (Fig. 2D). Per-seizure paired differences in mean z values reveal significantly greater SC-FC correlation during ictal periods than pre-ictal periods ($P = 0.023$, linear mixed effects analysis with subject as random effect). This effect was maintained when substituting pre-ictal periods with randomly chosen interictal clips of equivalent duration at least 6 h away from seizure activity ($P = 0.021$). It was also maintained after regressing out the effect of distance ($P < 0.05$, Supplementary Fig. 2). Moreover, there were no

Table 1 Patient demographic and clinical information, along with number of regions of interest included in analysis

Subject	Gender	Age of onset, years [epilepsy duration]	Age at MRI, years [at surgery]	Seizure frequency	MRI finding	Localization	Pathology	Treatment	Outcome	Seizures recorded (*n*)	Regions of interest
1	Female	20 [28]	47 [48]	FIAS: 2–3/week FBTC: 1–2/months	Non-lesional	RTL	HG	ATL + hippocampectomy	IA	FBTC (3)	84
2	Male	27 [12]	37 [39]	FAS: 1–day clusters, 1/months FBTC: 1/months	RTL cortical lesion, possible DNET	RTL/DNET	HG + MTS/HS + tumour	ATL + hippocampectomy	IB	FBTC (2)	55
3	Female	24 [21]	45 [45]	FAS: 2–4/week FIAS: ~1/week	Non-lesional	LTL	MTS/HS	ATL + hippocampectomy	IA	FIAS (1), FBTC (3)	116
4	Male	5 [31]	36 [36]	FIAS: 5–day clusters, 4/year FBTC: 2 in lifetime	Non-lesional	RTL	Gliosis + MTS/HS	ATL + hippocampectomy	IB	FAS (1), FIAS (5)	118
5	Female	29 [11]	39 [40]	FIAS: 1–2/months	Non-lesional	RTL	Gliosis + MTS/HS	ATL + hippocampectomy	IA	FIAS (5)	101
6	Male	28 [23]	50 [51]	FIAS: 3–5/months	Bilateral PVH	Bilateral PVH[a,b]	N/A	N/A	N/A	FIAS (4)	70
7	Male	4 [20]	24 [24]	FAS: 10–15/week FIAS: 7/week FBTC: 4/months	Non-lesional	RTL	Gliosis + MTS/HS	ATL + hippocampectomy	IB	FIAS (6)	90
8	Female	12 [46]	57 [58]	FIAS: 2–5/months	Non-lesional	BTL[a]	N/A	N/A	N/A	FIAS (5)	116
9	Female	22 [5]	23 [27]	FIAS: 3–5/week FBTC: 2 in lifetime	Non-lesional	LTL	N/A	Laser ablation	IA	FIAS (10)	111

Post-surgical outcome was based on Engel classification score (scale: I–IV, seizure freedom to no improvement).

[a]intracranial electrodes placed in both hemispheres for these two bilateral focal epilepsy patients.

[b]MRI revealed bilateral subependymal nodular heterotopias in bilateral temporal horns and atria of the lateral ventricles. On iEEG, one epileptogenic focus was identified in the left temporal region via a 6-contact strip electrode placed over the left anterior temporal lobe and an 8-contact depth electrode placed in the left PVH.

ATL = anterior temporal lobectomy; BTL = bilateral temporal lobe; DNET = dysembryoplastic neuroepithelial tumour; FAS = focal aware seizure; FBTC = focal to bilateral tonic-clonic seizure; FIAS = focal impaired awareness seizure; GTC = generalized tonic-clonic seizure; HG = hippocampal gliosis; HS = hippocampal sclerosis; LTL = left temporal lobe; MTS = mesial temporal sclerosis; N/A = not applicable; PVH = periventricular heterotopia; RTL = right temporal lobe.

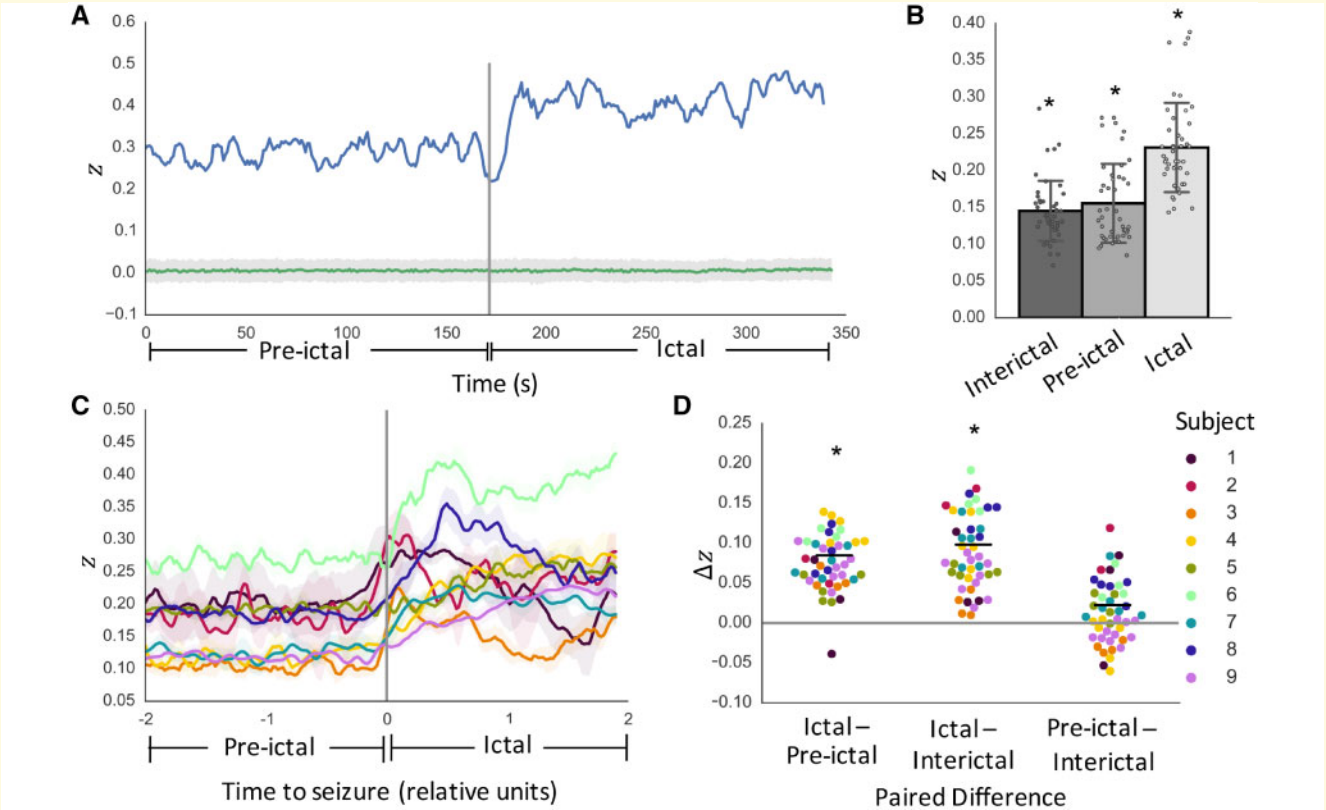

Figure 2 SC-FC analysis using broadband functional connectivity. (**A**) Temporal dynamics of SC-FC correlation as measured by Fisher's z for one example seizure in one patient, along with permutation-based null distribution of z values (mean ± standard deviation). (**B**) Per-seizure z-values during interictal, pre-ictal, and ictal periods reveal SC-FC correlations significantly greater than chance across all periods ($P < 0.05$). (**C**) Temporal dynamics of SC-FC correlation across all subjects (mean ± standard deviation across seizures in each subject). For visualization purposes only, time courses were normalized to span 200 evenly spaced time windows (100 pre-ictal and 100 ictal) and smoothed with a 5-window moving average filter. (**D**) Per-seizure paired differences in mean z-values reveal significantly greater SC-FC correlation during ictal periods than pre-ictal periods ($P = 0.023$). This effect holds when substituting pre-ictal periods with interictal periods ($P = 0.021$), with no significant difference between pre-ictal and interictal period SC-FC correlation values ($P = 0.70$). $^*P < 0.05$.

significant differences between pre-ictal and interictal period SC-FC correlation values ($P = 0.70$).

Frequency-specific SC-FC analysis

Next, to understand the frequency dependence of the observed increase in SC-FC coupling during seizures better, we repeated the SC-FC coupling analysis across four frequency bands (α/θ, β, low-γ, and high-γ). Similar to the previous analysis, we found that the extent of SC-FC coupling was significantly greater than chance at all time points during pre-ictal and ictal periods ($P < 0.05$, permutation-based testing) for all frequency bands (Fig. 3A). Moreover, while the pre-ictal SC-FC was lower in higher frequency bands (Fig. 3B), the increase in SC-FC coupling between pre-ictal and ictal periods was significant across all frequency bands (α/θ: $P < 0.05$; β: $P < 0.05$; low-γ: $P < 0.05$; high-γ: $P < 0.05$) (Fig. 3B and C). This finding was upheld after regressing out the effect of distance (Supplementary Fig. 2). Similar to the findings with broadband functional connectivity, the findings were consistent when substituting pre-ictal periods with interictal periods (α/θ: $P < 0.05$; β: $P < 0.05$; low-γ: $P < 0.05$; high-γ: $P < 0.05$), and there were no significant differences between pre-ictal and interictal period SC-FC correlation values (α/θ: $P > 0.05$; β: $P > 0.05$; low-γ: $P > 0.05$; high-γ: $P > 0.05$) (Supplementary Fig. 3).

We noted that while the increase was significant across all frequency bands, there were subject-specific frequency-dependent changes in SC-FC correlation. For example, Subject 4 exhibited particularly salient increases in $SC\text{-}FC_{high\text{-}\gamma}$ coupling, while Subject 6 had only moderate increases in $SC\text{-}FC_{high\text{-}\gamma}$ coupling but higher increases in $SC\text{-}FC_{\beta}$ and $SC\text{-}FC_{low\text{-}\gamma}$ (Fig. 3C and Supplementary Fig. 4). Finally, we characterized the within-subject similarity of the SC-FC time courses across all frequency bands. Using Euclidean distance as a measure of dissimilarity, we determined that the SC-FC time courses were significantly more similar within-patient than between-patient ($P < 0.001$, $R^2 = 0.50$, permutational MANOVA) (Fig.

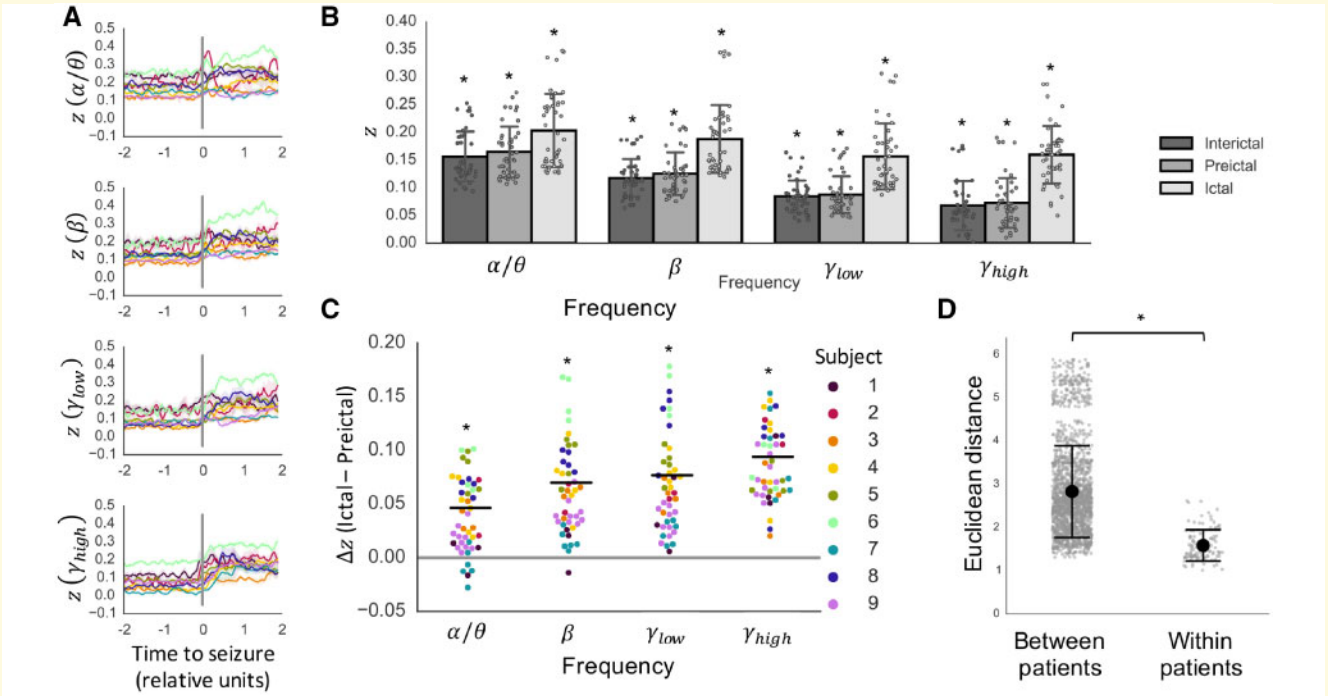

Figure 3 Frequency-specific SC-FC analysis. (**A**) Temporal dynamics of SC-FC correlation as measured by Fisher's z in α/θ, β, low-γ, and high-γ frequency bands (mean ± standard deviation across seizures in each subject, following interpolation to normalize ictal and pre-ictal durations). (**B**) Per-seizure z-values during interictal, pre-ictal, and ictal periods (mean ± SD) are significantly greater than chance ($P < 0.05$, permutation-based testing). (**C**) The increase in SC-FC correlation between pre-ictal and ictal periods is further illustrated using paired differences for each individual seizure ($P < 0.05$, linear mixed effects analysis with subject as random effect). (**D**) Seizures within subjects evolve similarly, as evidenced by higher between-patient Euclidean distances between SC-FC correlation time courses compared to within-patient distances ($P < 0.001$, $R^2 = 0.50$, PERMANOVA). *$P < 0.05$.

3D), indicating that the temporal dynamics of SC-FC coupling is stereotyped in each patient across seizure events.

SC-FC analysis during postictal periods

To understand whether the observed increase in SC-FC coupling during seizures persists postictally, we repeated the SC-FC coupling analysis using iEEG data obtained from the first 5 min following seizure termination. Although time courses varied across seizures, we observed three distinct patterns of postictal SC-FC coupling as follows: (i) SC-FC coupling persisted, but did not increase, in the immediate postictal period and subsequently decreased; (ii) SC-FC coupling increased into the immediate postictal period and later decreased; and (iii) SC-FC coupling decreased sharply at or prior to the start of the postictal period (Fig. 4A). Generally, SC-FC coupling ultimately decreased during the postictal period, though not always to the level of SC-FC coupling in the pre-ictal period. Given the different pattern during the immediate postictal period (usually up to 1 min following seizure termination), we separated the postictal period into immediate (Minutes 0–1) and later (Minutes 1–5) subperiods. Per-seizure paired differences in mean *z*-values revealed significant decreases in SC-FC coupling between ictal periods and later postictal periods across all tested frequency bands, while significant differences between SC-FC coupling between ictal periods and immediate postictal (Minutes 0–1) periods occurred only in α/θ and β frequency bands. ($P < 0.05$, linear mixed effects analysis with subject as random effect) (Fig. 4B).

SC-FC subanalysis in focal to bilateral tonic-clonic seizures

As noted previously, the temporal progression of SC-FC changes was subject-specific (Figs 2C and 3A). More specifically, we observed that in patients who experienced focal to bilateral tonic-clonic seizures (Subjects 1–3), there was a drop in SC-FC coupling after the initial rise following seizure onset. Analysis of the individual SC-FC time courses in these seizures revealed that the drop corresponded with onset of bilateral tonic-clonic activity (Fig. 5A). Furthermore, quantitative analysis revealed significantly greater SC-FC correlation during pre-bilateral tonic-clonic ictal periods than pre-ictal periods ($P < 0.05$), as well as significantly greater SC-FC correlation during pre-bilateral tonic-clonic ictal periods than post-bilateral tonic-clonic ictal periods ($P < 0.05$) (Fig. 5B). To focus

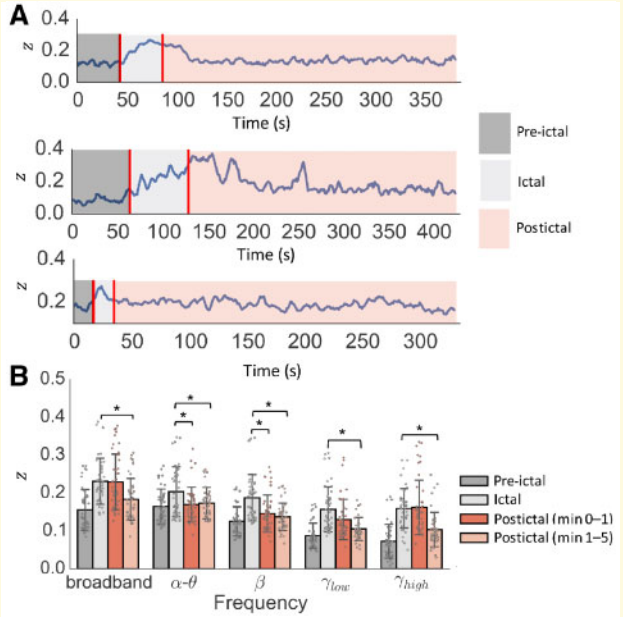

Figure 4 Assessment of SC-FC coupling in postictal periods. (**A**) Illustration of broadband SC-FC coupling across pre-ictal, ictal, and postictal periods, in three example seizures. Each represents one of three observed distinct patterns of post-ictal SC-FC coupling: (*top*) SC-FC coupling persists, but does not increase, in the immediate postictal period and subsequently decreases, (*middle*) SC-FC coupling increases into the immediate postictal period and later decreases, and (*bottom*) SC-FC coupling decreases sharply at or prior to the start of the postical period. (**B**) Per-seizure paired differences in mean z-values reveal significant decreases in SC-FC coupling between ictal periods and later postictal (Minutes 1–5) periods across all tested frequency bands, with significant differences between SC-FC coupling between ictal periods and immediate postictal (Minutes 0–1) periods occurring only in α/θ and β frequency bands. ($P < 0.05$, linear mixed effects analysis with subject as random effect). Pre-ictal period bars included for reference. $^{*}P < 0.05$.

on the relationship between structure and function prior to the onset of generalized hypersynchronous activity, we limited the ictal periods to the periods prior to bilateral tonic-clonic onset for the subsequent virtual edge resection analysis.

Virtual edge resection analysis

Given our finding that SC-FC coupling was significantly higher during ictal periods compared with pre-ictal periods, we wanted to identify and characterize the structural edges that statistically accounted for this increase. After quantifying the contribution $\sigma(i)$ of each edge on the SC-FC coupling, we mapped the contributor edges onto each subject's brain (Fig. 6) to facilitate subject-specific characterization of SC-FC relationships. Furthermore, at the group level, we determined that contributor edges were predominantly short-range, as quantified by significantly shorter edge lengths in contributors compared with non-contributors, based on both Euclidean distance ($P < 0.05$, two-tailed paired *t*-test) (Fig. 7A) and streamline distance ($P < 0.05$, two-tailed paired *t*-test) (Fig. 7B). This finding held individually for each subject. Within the contributor edges, we found within each subject that higher contribution edges are shorter-range, both in terms of Euclidean distance (Fig. 7C) and streamline length (Fig. 7D), with significant differences between low and medium contribution edges ($P < 0.05$, two-tailed paired *t*-test), and low and high contribution edges ($P < 0.05$, two-tailed paired *t*-test). These findings held following distance regression (Supplementary Fig. 2). When relating edge contributions to changes in functional connectivity, we found no significant correlation (Pearson $r = -0.04 \pm 0.13$; $P > 0.05$) (Supplementary Fig. 7A). While the edges with the largest changes in functional connectivity were typically short-range, these edges were often not the same as those with high contribution; moreover, many longer-range connections also exhibited significant increases in functional connectivity (Supplementary Fig. 7B *cf.* Fig. 6).

Global and local structural properties analysis

We analysed global structural network properties in our patient population and compared them to those of healthy controls. We found no significant difference in normalized clustering, (patients: 11.9 ± 1.31; controls: 11.0 ± 1.53; $P > 0.05$), normalized efficiency (patients: 0.80 ± 0.012; controls: 0.79 ± 0.020; $P > 0.05$), or small-worldness (patients: 9.43 ± 0.93; controls: 8.60 ± 1.08; $P > 0.05$) (Supplementary Fig. 5). We also correlated microstructural measures with both nodal SC-FC contribution and nodal FC change across regions of interest in each subject. We found no significant correlation between nodal contribution and mean FA ($r = 0.087 \pm 0.15$; $P > 0.05$) or mean MD ($r = -0.087 \pm 0.13$; $P > 0.05$). Similarly, we found no significant correlation between nodal functional connectivity change and mean MD ($r = 0.09 \pm 0.15$; $P > 0.05$). There was a mild but significant correlation between nodal functional connectivity change and mean FA ($r = 0.13 \pm 0.06$; $P < 0.05$) (Supplementary Fig. 6).

Discussion

The main goal of this study is to characterize the relationship between structural and functional connectivity during seizure onset and spread. Using network-based analysis of HARDI and iEEG data, we observe significant structure-function coupling at rest and a marked increase in this coupling during the progression from pre-ictal to ictal states. This finding persists across frequency bands, with subject-specific levels of frequency-dependent increases. Furthermore, we present a technique for assessing the impact of individual structural connections to the observed ictal increase in structure-function correlation, and

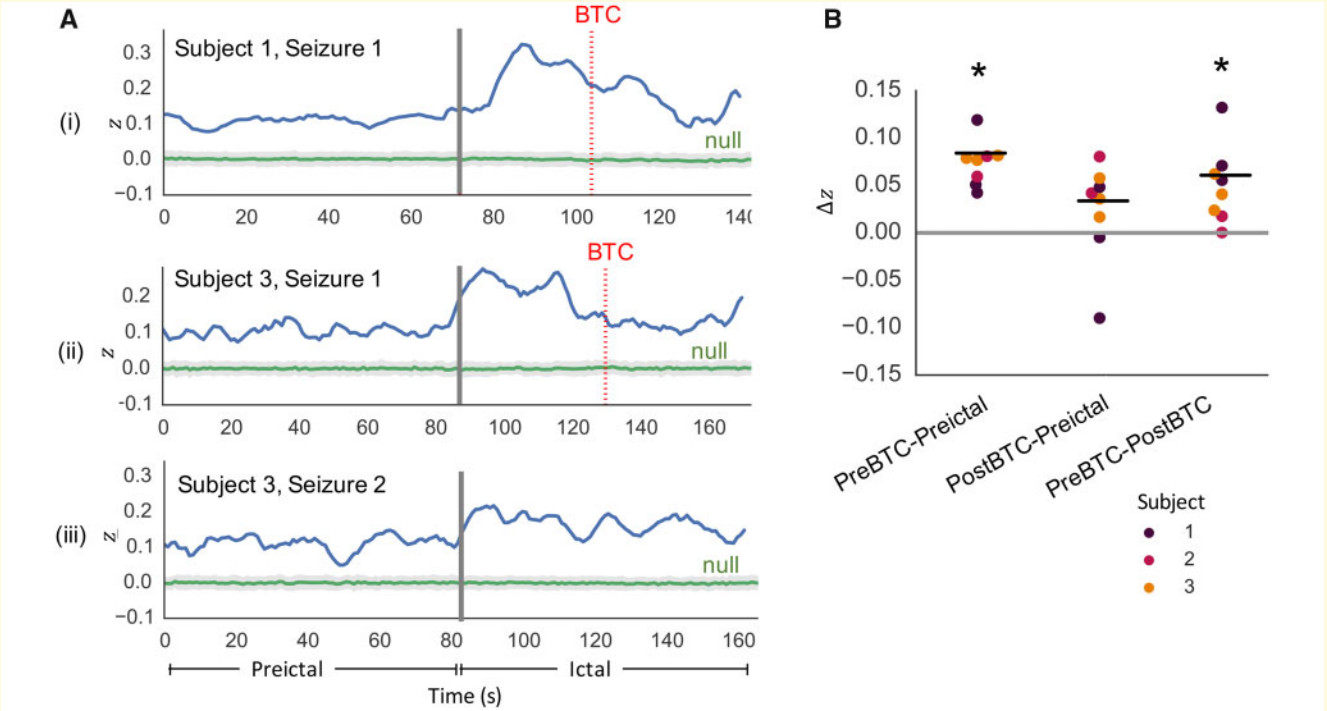

Figure 5 Assessment of SC-FC coupling in focal to bilateral tonic-clonic seizures. (**A**) Illustration of SC-FC coupling in two focal to bilateral tonic-clonic seizures, one from Subject 1 and one from Subject 3, reveals decrease in SC-FC coupling following bilateral tonic-clonic (BTC) onset (bilateral tonic-clonic onset indicated by dotted red line). For comparison, SC-FC coupling time course from a focal impaired awareness seizure in Subject 3 (without bilateral tonic-clonic) does not illustrate the same decrease. (**B**) In all bilateral tonic-clonic seizures, per-seizure paired differences in mean z-values reveal significantly greater SC-FC correlation during pre-bilateral tonic-clonic ictal periods than pre-ictal periods ($P < 0.05$), as well as significantly greater SC-FC correlation during pre-bilateral tonic-clonic ictal periods than post-bilateral tonic-clonic ictal periods ($P < 0.05$). $^{*}P < 0.05$.

demonstrate that the effect is primarily due to short-range connections. The consistency of findings across seizures within each patient suggests that the spatiotemporal patterns of structure-function coupling are highly stereotyped. Our findings shed light on the dynamics of focal epileptic seizures in relation to underlying structure by demonstrating that seizure spread is tightly controlled by short-range structural connections.

Structure-function coupling across time, frequency and space

We observe greater coupling between structural and broadband functional networks during pre-ictal and interictal periods than expected by chance. This finding is consistent with studies relating DTI-based structural networks to resting-state functional MRI-based functional networks in healthy adults (Skudlarski *et al.*, 2008; Damoiseaux and Greicius, 2009; Honey *et al.*, 2009; van den Heuvel *et al.*, 2009; Zhang *et al.*, 2010; Hermundstad *et al.*, 2013). It is important to note that the functional signals recorded using iEEG are fundamentally different from those recorded using functional MRI. While recent studies suggest that blood oxygen level-dependent (BOLD) signal fluctuations correlate with slow fluctuations in EEG gamma power, the exact relationship between functional MRI (BOLD) signals and electrophysiology has yet to be resolved (Logothetis *et al.*, 2001; He and Liu, 2008; He and Raichle, 2009; Ko *et al.*, 2011) Nonetheless, our finding suggests that the tie between structure and function at rest is robust across diverse measurements of functional connectivity.

Interestingly, we observe that pre-ictal functional connectivity networks in lower frequency bands have higher correlation to structural connectivity networks than pre-ictal functional connectivity networks in higher frequency bands. This relationship decreases during the ictal period, with high SC-FC coupling in all frequency bands. Since it is believed that lower frequencies facilitate long-distance connections in the brain while higher frequencies facilitate shorter connections (Kopell *et al.*, 2000; Miller *et al.*, 2007), our findings may suggest a relative shift to short-range, high-frequency connectivity during seizure generation. However, this observation could be influenced by the spatial distribution of electrodes, which tend to be clustered around the putative seizure onset zone, leading to a bias towards short-range connections within the seizure

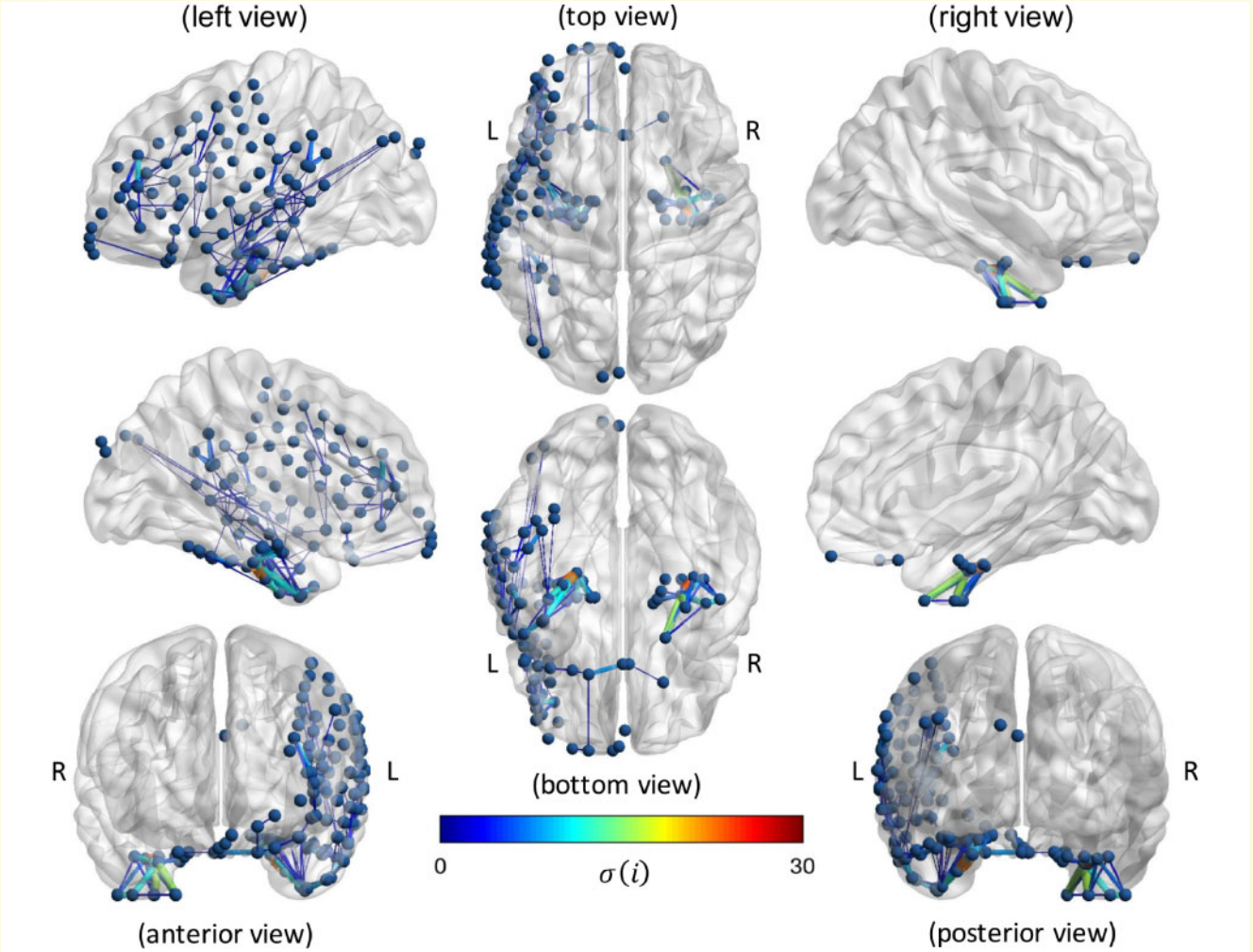

Figure 6 Subject-specific virtual edge resection approach to determine the contribution, $\sigma(i)$, of each structural edge i on the increase in SC-FC correlation during seizures. Results are shown for an example seizure in a patient with left temporal lobe epilepsy. Only 'contributor' edges [$\sigma(i) > 0$ and $\Delta z_{ictal}(i) > 0$] are included to highlight edges that are associated with the SC-FC increase, with edge thickness and colour used to representing magnitude of $\sigma(i)$.

generating network. Therefore, we plan to corroborate these findings in patients with stereo-EEG, an increasingly popular and less invasive method that records from stereotactically-placed intracranial depth electrodes (Cossu *et al.*, 2005; Varotto *et al.*, 2012; Luders *et al.*, 2013). In comparison to the depth electrodes used to sample the hippocampus and amygdala alongside strips and grids in our study's patients, stereo-EEG electrodes are more flexible to allow for stereotactic placement. More importantly, because of the ability to place stereo-EEG electrodes without large, highly-invasive craniotomies, stereo-EEG allows for bilateral electrode placement within multiple deep cortical structures and overlying cortex, as well as sampling from multiple non-contiguous lobes (Gonzalez-Martinez *et al.*, 2013). Therefore, stereo-EEG may allow us to sample more regions of the brain and capture longer-range connections.

Despite individual variations inherent to our patient population, the finding of increased SC-FC coupling during ictal periods compared with pre-ictal periods is extremely robust, using both broadband and narrow-band functional connectivity. We compared SC-FC time courses from ictal periods to those of immediately pre-ictal periods to allow for matched pairwise comparisons and to facilitate visualization along a continuous temporal scale. To ensure that activity immediately prior to seizure onset is a good representation of non-ictal activity, we repeated our analysis after substituting the pre-ictal periods with interictal periods far away from seizure activity, and attain consistent results. The rise in SC-FC coupling during seizures indicates that seizures may rely on the brain's underlying architecture during initial seizure spread. We note that in several of the patients, the rise in SC-FC correlation occurs prior to the clinically-marked earliest electrographic change

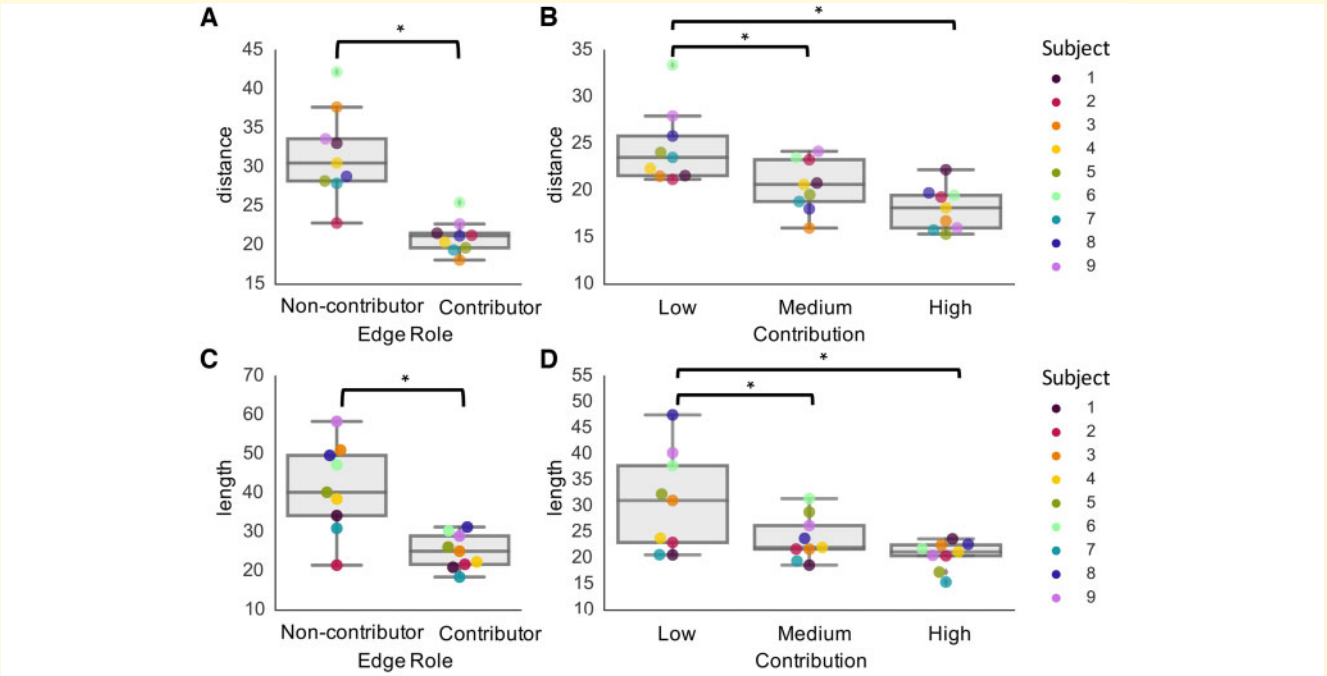

Figure 7 Relationship between edge contribution and edge length. Findings reveal that contributor edges are shorter-range in terms of both (**A**) Euclidean distance and (**C**) streamline length ($P < 0.05$, two-tailed paired *t*-test). Furthermore, there is a trend that edges with higher contribution are shorter-range, in terms of both (**B**) Euclidean distance and (**D**) streamline length, with significant differences between low and medium contribution edges ($P < 0.05$, two-tailed paired *t*-test), and low and high contribution edges ($P < 0.05$, two-tailed paired *t*-test). $^{*}P < 0.05$.

representative of seizure onset, suggesting that SC-FC coupling may also be a valuable biomarker for seizure prediction or its early generation.

We observed that the only two bilateral focal epilepsy patients, Subjects 6 and 8, had the highest Fisher's *z*-values across pre-ictal and ictal periods in all frequency bands, and highest Δz-values in all bands except high gamma. This observation suggests that the extent of structure-function coupling changes may be dependent on the extent of alterations in the underlying seizure network. However, there are clearly a number of factors that may be involved, including the location and extent of tissue involved. Therefore, this observation could be explored in future larger-scale studies with patients of both bilateral and unilateral onset, accounting for possible covariates.

We find that the pattern of SC-FC coupling during the postictal period varies across seizures. In some seizures, there is an initial persistence or increase in SC-FC coupling in the immediate postictal period followed by a decrease, while in some seizures, SC-FC coupling decreases immediately. While the postictal EEG is often characterized by slowing and suppression—particularly in focal to bilateral tonic-clonic seizures—the dynamics of the postictal period are variable, complex, and poorly understood (Kaibara and Blume, 1988; Bateman *et al.*, 2019; Marchi *et al.*, 2019). Additionally, the transition from ictal to postictal is known to be ambiguous, as the end of a seizure is often not well demarcated, neither clinically nor electrophysiologically (Fisher and Engel, 2010). Therefore, our finding of persistence of SC-FC coupling during the first minute following seizure termination may be a consequence of the imprecise boundary between seizure and post-seizure. Additionally, the observation that the degree of postictal SC-FC coupling is higher than that of the pre-ictal period may be due to the fact that postictal EEG can take hours to days to return to baseline (Litt *et al.*, 2001; Fisher and Engel, 2010; So and Blume, 2010). Further studies should be carried out to better understand the dynamics of functional connectivity and structure-function relationships over longer postictal time scales.

We discover that in focal to bilateral tonic-clonic seizures, there is a significant decrease in SC-FC coupling after the onset of bilateral tonic-clonic activity. This finding is not surprising, given that bilateral tonic-clonic periods are associated with generalized hypersynchronous neural activity that is not localized to particular brain regions or pathways. This finding also supports that the observed SC-FC coupling increase during seizures relates to seizure propagation, and is not simply a result of highly synchronous activity.

Of note, the temporal dynamics of SC-FC coupling is highly consistent between seizures within each patient. This indicates that seizures may be 'hard-wired' in a sense, and is a macroscopic analogue to the microscale finding of stereotyped ictal progression (Wenzel *et al.*, 2017). However, since our dataset consists of a relatively

small group of adult focal epilepsy patients, with the majority having temporal lobe epilepsy, these conclusions may be specific to our dataset and should be confirmed using larger, more diverse patient populations.

To assess the role of each structural connection on the rise in SC-FC coupling during seizures, we implement a virtual edge resection method. Such leave-one-out simulation-based methods have been gaining popularity to probe the role of individual nodes and edges on overall network topology (Honey and Sporns, 2008; Alstott *et al.*, 2009; Rafal *et al.*, 2015; Khambhati *et al.*, 2016). In our case, we determine the contribution of structural connections to SC-FC correlation and generate seizure-specific brain maps of these connections. Group-level analysis reveals that connections with high contribution are predominantly short-range, in terms of both streamline length and Euclidean distance. Of note, the distributions of all streamline lengths (including both contributors and non-contributors) are skewed to the right, indicating that the majority of structural edges are relatively short range. This is due to two phenomena. First, prior studies have demonstrated the brain consists of a large number of short connections and few long-range connections to minimize wiring cost while allowing for efficient communication (Klyachko and Stevens, 2003; Chen *et al.*, 2006; Hagmann *et al.*, 2007). Second, since structural connections analysed in this study are based on electrode locations, and the electrodes are typically clustered around the putative seizure onset location rather than distributed throughout the brain, this leads to a further bias towards shorter range connections. Nonetheless, we see that the edges contributing to SC-FC coupling are statistically shorter than the non-contributors, and that stronger contributors are even shorter-range, indicating that our findings are not simply due to selection of local networks. Interestingly, edge contribution was not significantly correlated to change in functional connectivity. This suggests that our finding of edge contribution is not simply a consequence of functional connectivity changes, and the relationship between functional seizure spread and edge contribution is more complex.

We found no significant differences in global structural network properties between our patient population and healthy controls. Moreover, we found that the observed increases in SC-FC coupling from pre-ictal to ictal periods are not significantly correlated to microstructural properties such as fractional anisotropy and mean diffusivity. This could be partly due to our patient population, which consisted primarily of subjects with no clear lesion on MRI (though several exhibited signs of hippocampal sclerosis on subsequent pathology). Additionally, these findings suggest that multimodal connectivity-based analysis captures unique information about seizure dynamics that are not evident from standard structural image analyses. We plan to repeat our findings in larger datasets to corroborate our observations. Furthermore, further studies in MRI-lesional patient datasets should be undertaken to relate SC-FC coupling changes to the anatomical location and extent of structural lesions.

While the connections themselves are short, the locations of these connections appear distributed across the brain, including connections that are contralateral to seizure onset. This suggests that seizure dynamics rely on a distributed network of locally clustered connections. While further analyses and validation are needed, mapping connections in relation to seizure onset and spread could ultimately be useful in pinpointing networks for therapeutic removal via targeted methods such as laser ablation (Willie *et al.*, 2014) or neurostimulation (Fisher and Velasco, 2014).

Methodological considerations and limitations

An important but inevitable limitation of this work relates to the incomplete sampling of the network via iEEG. Electrode placement is limited by clinical necessity and constrained by the boundaries of the craniotomy, in order to minimize invasiveness and reduce patient morbidity. Therefore, it is not possible to sample functional connectivity from the entire brain at high resolution time scales accessible through iEEG. While clinicians aim to place electrodes around putative seizure onset zones, it is possible that the entire seizure network may not be captured in certain cases. Recent efforts to map whole-brain iEEG using recordings from multiple subjects (Betzel *et al.*, 2017) and to construct models of whole-brain iEEG within individual subjects (Owen and Manning, 2017) may help circumvent this issue. Furthermore, while limited by impedance from the skull and inability to localize subcortical activity, ictal scalp EEG recordings, or ictal MEG recordings could supplement our intracranial analysis as both allow for consistent, grid-like spatial sampling with temporal resolution comparable to iEEG. The feasibility of such approaches has already been demonstrated in a recent paper revealing significant overlap between DTI networks and scalp EEG functional networks in the interictal state (Chu *et al.*, 2015), and in early work on ictal MEG.

Another consideration lies in the method of establishing correspondence between functional network nodes and structural network nodes. We chose to make the assignment based on anatomical location of the electrode centroids. This decision was based on prior research demonstrating that the field created by neurons more than 1 cm away from an electrode contributes minimally to the recorded signal, and that the weight of contribution of a brain signal source is inversely proportional to the square of the distance separating the source from the electrode contact (Morris and Lüders, 1985; Lachaux *et al.*, 2003). Therefore, it is reasonable to assume that the majority of signal recorded by an iEEG electrode likely arises from neighbouring brain tissue. Nonetheless, it is possible that a strong signal from a remote location can contribute

the recorded signal. In scalp EEG and MEG studies, source localization methods are often used to circumvent this issue by locating signal sources (Cohen *et al.*, 1990; Mosher and Leahy, 1998). However, while source localization in intracranial EEG has been investigated, it is not commonly used because of many unknowns, such as the number of iEEG electrodes needed for reconstruction, the model to be used for the sources, and the volume conduction properties of the brain tissue (Lachaux *et al.*, 2003). More generally, because of the lack of unique solution to the inverse problem and the wide variety of modelling methods (Plummer *et al.*, 2008; Zhang *et al.*, 2008; Caune *et al.*, 2014), the reliability of the methodology should be explored further prior to incorporating it into our approach.

Our structural network findings are also limited by the capacity of our imaging methods. While HARDI has demonstrated superiority over conventional DTI in terms of its ability to resolve crossing fibres in regions of high fibre heterogeneity (Tuch *et al.*, 2002), HARDI tractography is still only a proxy for true white matter pathways. Similar to other neuroimaging modalities, it is subject to partial volume effects and artefacts such as eddy current and susceptibility distortions (Le Bihan *et al.*, 2006; Assaf and Pasternak, 2008). Diffusion-based tractography is documented to recapitulate known pathways types including the short and long association fibres linking cortical gyri, the projection fibre connecting the cortex to lower portions of the brain, and the commissural fibres linking the two hemispheres (Mamata *et al.*, 2002), but may not reconstruct unmyelinated intracortical axons. Furthermore, streamline count may not be a direct measure of the strength of anatomical connectivity.

We decided to include medically-refractory patients with a range of clinical findings (in terms of laterality, lesional status, and seizure types) in our study, rather than restricting to a particular subtype epilepsy. Notably, our findings were robust across patients despite heterogeneity. While we included one patient with periventricular nodular heterotopia (PVH), a malformation of cortical development, histological evidence suggests that these patients manifest with an altered arrangement of fibre tracks and microstructural abnormalities beyond visible lesions that may displace the axonal tracts from their expected location (Kakita *et al.*, 2005; Meroni *et al.*, 2009; Liu *et al.*, 2017). Therefore, in future work, the anatomical locations of salient structure-function changes should be analysed carefully in the context of these alterations.

Because of the strong relationship between spatial proximity and structural connection strength, it is not possible to entirely disentangle the effects of Euclidean distance on our findings. Given prior work that epileptiform activity propagates within layer V of the neocortex (Badawy *et al.*, 2009), it is possible that local functional connections could partially be attributed to local cortical spreading phenomena rather than white matter propagation along short-range arcuate fibres. Local functional connectivity could also be due to measurement of a common source of signal. Despite these concerns, our finding of higher SC-FC coupling during seizures hold after regressing out Euclidean distance from our structural networks. This suggests that SC-FC coupling goes beyond solely distance-based effects.

Finally, while this study considers only direct structural connections, functional connectivity in the brain is also partially attributed to indirect structural connections (Damoiseaux and Greicius, 2009; Honey *et al.*, 2009; Liang *et al.*, 2017). Future studies could use the property of communicability (Estrada and Hatano, 2008) to incorporate path lengths of greater than one into the construction of structural networks while also accounting for the effects of spatial proximity.

Conclusions

We present a comprehensive approach to understanding the relationship between structure and function in the epileptic brain. Our work provides important insights into the structural underpinnings of seizure dynamics. Our network analysis scripts, associated visualizations, and data are publicly available at https://github.com/shahpreya/EpiConn. It is our hope that by openly sharing our data, code and pipeline that we can accelerate translating this nascent field of network analysis in clinical epilepsy to help patients.

Funding

This work was supported by National Institutes of Health grants 1R01NS099348, K23-NS073801, 1R01NS085211, and 1R01MH112847. We also acknowledge support by the Thornton Foundation, the Mirowski Family Foundation, the ISI Foundation, the John D. and Catherine T. MacArthur Foundation, the Sloan Foundation, and the Paul Allen Foundation.

Competing interests

The authors report no competing interests.

Supplementary material

Supplementary material is available at *Brain* online.

References

Alstott J, Breakspear M, Hagmann P, Cammoun L, Sporns O. Modeling the Impact of Lesions in the Human Brain. PLoS Comput Biol 2009; 5: e1000408.

Anderson MJ. Permutational multivariate analysis of variance (PERMANOVA). In: Wiley StatsRef: Statistics Reference Online. Chichester, UK: John Wiley & Sons, Ltd; 2017. p. 1–15.

Andersson JLR, Sotiropoulos SN. An integrated approach to correction for off-resonance effects and subject movement in diffusion MR imaging. Neuroimage 2016; 125: 1063–78.
Assaf Y, Pasternak O. Diffusion tensor imaging (DTI)-based white matter mapping in brain research: a review. J Mol Neurosci 2008; 34: 51–61.
Avants B, Tustison N, Song G. Advanced Normalization Tools (ANTS). Insight J. 2009; 2: 1–35.
Avants BB, Epstein CL, Grossman M, Gee JC. Symmetric diffeomorphic image registration with cross-correlation: evaluating automated labeling of elderly and neurodegenerative brain. Med Image Anal 2008; 12: 26–41.
Avants BB, Tustison NJ, Song G, Cook PA, Klein A, Gee JC. A reproducible evaluation of ANTs similarity metric performance in brain image registration. Neuroimage 2011; 54: 2033–44.
Badawy RAB, Harvey AS, Macdonell RAL. Cortical hyperexcitability and epileptogenesis: Understanding the mechanisms of epilepsy - Part 2. J Clin Neurosci 2009; 16: 485–500.
Bassett DS, Bullmore ET. Small-World Brain Networks Revisited. Neuroscientist 2017; 23: 499–516.
Bassett DS, Sporns O. Network neuroscience. Nat Neurosci 2017; 20: 353–64.
Bateman LM, Mendiratta A, Liou J-Y, Smith EJ, Bazil CW, Choi H, et al. Postictal clinical and electroencephalographic activity following intracranially recorded bilateral tonic-clonic seizures. Epilepsia 2019; 60: 74–84.
Bernasconi A. Connectome-based models of the epileptogenic network: a step towards epileptomics? Brain 2017; 140: 2525–7.
Bernhardt BC, Hong S, Bernasconi A, Bernasconi N. Imaging structural and functional brain networks in temporal lobe epilepsy. Front Hum Neurosci 2013; 7: 624.
Betzel RF, Medaglia JD, Kahn AE, Soffer J, Schonhaut DR, Bassett DS. Inter-regional ECoG correlations predicted by communication dynamics, geometry, and correlated gene expression [Internet]. arXiv.org 2017 [cited 2018 Sep 4]. Available from: https://arxiv.org/abs/1706.06088.
Le Bihan D, Poupon C, Amadon A, Lethimonnier F. Artifacts and pitfalls in diffusion MRI. J. Magn Reson Imaging 2006; 24: 478–88.
Biswal B, Zerrin Yetkin F, Haughton VM, Hyde JS. Functional connectivity in the motor cortex of resting human brain using echo-planar MRI. Magn Reson Med 1995; 34: 537–41.
Bonilha L, Gleichgerrcht E, Nesland T, Rorden C, Fridriksson J. Gray matter axonal connectivity maps. Front Psychiatry 2015; 6: 35.
Bullmore E, Sporns O. Complex brain networks: graph theoretical analysis of structural and functional systems. Nat Rev Neurosci 2009; 10: 186–98.
Burns SP, Santaniello S, Yaffe RB, Jouny CC, Crone NE, Bergey GK, et al. Network dynamics of the brain and influence of the epileptic seizure onset zone. Proc Natl Acad Sci 2014; 111: E5321–30.
de Campos BM, Coan AC, Lin Yasuda C, Casseb RF, Cendes F. Large-scale brain networks are distinctly affected in right and left mesial temporal lobe epilepsy. Hum Brain Mapp 2016; 37: 3137–52.
Caune V, Ranta R, Le Cam S, Hofmanis J, Maillard L, Koessler L, et al. Evaluating dipolar source localization feasibility from intracerebral SEEG recordings. Neuroimage 2014; 98: 118–33.
Chen BL, Hall DH, Chklovskii DB. Wiring optimization can relate neuronal structure and function. Proc Natl Acad Sci USA 2006; 103: 4723–8.
Chiang S, Stern JM, Engel J, Haneef Z. Structural-functional coupling changes in temporal lobe epilepsy. Brain Res 2015; 1616: 45–57.
Chu CJ, Tanaka N, Diaz J, Edlow BL, Wu O, Hämäläinen M, et al. EEG functional connectivity is partially predicted by underlying white matter connectivity. Neuroimage 2015; 108: 23–33.
Cohen D, Cuffin BN, Yunokuchi K, Maniewski R, Purcell C, Cosgrove GR, et al. MEG versus EEG localization test using implanted sources in the human brain. Ann Neurol 1990; 28: 811–7.
Cossu M, Cardinale F, Castana L, Citterio A, Francione S, Tassi L, et al. Stereoelectroencephalography in the presurgical evaluation of focal epilepsy: a retrospective analysis of 215 procedures. Neurosurgery 2005; 57: 706–18.
Damoiseaux JS, Greicius MD. Greater than the sum of its parts: a review of studies combining structural connectivity and resting-state functional connectivity. Brain Struct Funct 2009; 213: 525–33.
Davison AC, Hinkley DV. Bootstrap methods and their application. Technometrics 1997: 582.
Donahue CJ, Sotiropoulos SN, Jbabdi S, Hernandez-Fernandez M, Behrens TE, Dyrby TB, et al. Using diffusion tractography to predict cortical connection strength and distance: a quantitative comparison with tracers in the monkey. J Neurosci 2016; 36: 6758–70.
Estrada E, Hatano N. Communicability in complex networks. Phys Rev E - Stat Nonlin Soft Matter Phys 2008; 77: 036111.
Fazel S, Wolf A, Långström N, Newton CR, Lichtenstein P. Premature mortality in epilepsy and the role of psychiatric comorbidity: a total population study. Lancet (London, England) 2013; 382: 1646–54.
Finger H, Bönstrup M, Cheng B, Messé A, Hilgetag C, Thomalla G, et al. Modeling of large-scale functional brain networks based on structural connectivity from DTI: comparison with EEG derived phase coupling networks and evaluation of alternative methods along the modeling path. PLoS Comput Biol 2016; 12: e1005025.
Fisher RA. On the 'probable error' of a coefficient of correlation deduced from a small sample. Metron 1921; 1: 3–32.
Fisher RS, Cross JH, Souza CD', French JA, Haut SR, Higurashi N, et al. Instruction manual for the ILAE 2017 operational classification of seizure types. Epilepsia 2017; 58: 531–42.
Fisher RS, Engel JJ. Definition of the postictal state: When does it start and end? Epilepsy Behav 2010; 19: 100–4.
Fisher RS, Velasco AL. Electrical brain stimulation for epilepsy. Nat Rev Neurol 2014; 10: 261–70.
French JA. Refractory epilepsy: clinical overview. Epilepsia 2007; 48: 3–7.
Gonzalez-Martinez J, Bulacio J, Alexopoulos A, Jehi L, Bingaman W, Najm I. Stereoelectroencephalography in the 'difficult to localize' refractory focal epilepsy: early experience from a North American epilepsy center. Epilepsia 2013; 54: 323–30.
Goodfellow M, Rummel C, Abela E, Richardson MP, Schindler K, Terry JR. Estimation of brain network ictogenicity predicts outcome from epilepsy surgery. Sci Rep 2016; 6: 29215.
Greicius, Supekar, Menon, Dougherty. Resting-state functional connectivity reflects structural connectivity in the default mode network. Cereb Cortex 2009; 19: 72–8.
Greve DN, Fischl B. Accurate and robust brain image alignment using boundary-based registration. Neuroimage 2009; 48: 63–72.
Hagmann P, Cammoun L, Gigandet X, Meuli R, Honey CJ, Wedeen VJ, et al. Mapping the structural core of human cerebral cortex. PLoS Biol 2008; 6: e159.
Hagmann P, Kurant M, Gigandet X, Thiran P, Wedeen VJ, Meuli R, et al. Mapping human whole-brain structural networks with diffusion MRI. PLoS One 2007; 2: e597.
Hagmann P, Sporns O, Madan N, Cammoun L, Pienaar R, Wedeen VJ, et al. White matter maturation reshapes structural connectivity in the late developing human brain. Proc Natl Acad Sci USA 2010; 107: 19067–72.
Halekoh U, Højsgaard S. A Kenward-Roger approximation and parametric bootstrap methods for tests in linear mixed models - The R package pbkrtest. J Stat Softw 2014; 59: 1–32.
He B, Liu Z. Multimodal functional neuroimaging: integrating functional MRI and EEG/MEG. IEEE Rev Biomed Eng 2008; 1: 23–40.
He BJ, Raichle ME. The fMRI signal, slow cortical potential and consciousness. Trends Cogn Sci 2009; 13: 302–9.
Hermundstad AM, Bassett DS, Brown KS, Aminoff EM, Clewett D, Freeman S, et al. Structural foundations of resting-state and task-based functional connectivity in the human brain. Proc Natl Acad Sci 2013; 110: 6169–74.

Hermundstad AM, Brown KS, Bassett DS, Aminoff EM, Frithsen A, Johnson A, et al. Structurally-Constrained Relationships between Cognitive States in the Human Brain. PLoS Comput Biol 2014; 10: e1003591.

Hesdorffer DC, Logroscino G, Benn EKT, Katri N, Cascino G, Hauser WA. Estimating risk for developing epilepsy: a population-based study in Rochester, Minnesota. Neurology 2011; 76: 23–7.

van den Heuvel MP, Mandl RCW, Kahn RS, Hulshoff Pol HE. Functionally linked resting-state networks reflect the underlying structural connectivity architecture of the human brain. Hum Brain Mapp 2009; 30: 3127–41.

Honey CJ, Sporns O. Dynamical consequences of lesions in cortical networks. Hum Brain Mapp 2008; 29: 802–9.

Honey CJ, Sporns O, Cammoun L, Gigandet X, Thiran JP, Meuli R, et al. Predicting human resting-state functional connectivity from structural connectivity. Proc Natl Acad Sci USA 2009; 106: 2035–40.

Hussan SM, Christian BK, David DL, Karen S-M, Robert LGJ, Steven MR, et al. Impact of epilepsy on seizure control and quality of life: a 26-year follow-up study. Epilepsia 2012; 53: 712–20.

Jette N, Wiebe S. Update on the surgical treatment of epilepsy. Curr Opin Neurol 2013; 26: 201–7.

Jirsa VK, Proix T, Perdikis D, Woodman MM, Wang H, Gonzalez-Martinez J, et al. The virtual epileptic patient: individualized whole-brain models of epilepsy spread. Neuroimage 2017; 145: 377–88.

Kaibara M, Blume WT. The postictal electroencephalogram. Electroencephalogr Clin Neurophysiol 1988; 70: 99–104.

Kaiser M, Hilgetag CC. Modelling the development of cortical systems networks. Neurocomputing 2004; 58–60: 297–302.

Kakita A, Kameyama S, Hayashi S, Masuda H, Takahashi H. Pathologic features of dysplasia and accompanying alterations observed in surgical specimens from patients with intractable epilepsy. J Child Neurol 2005; 20: 341–50.

Khambhati AN, Bassett DS, Oommen BS, Chen SH, Lucas TH, Davis KA, et al. Recurring functional interactions predict network architecture of interictal and ictal states in neocortical epilepsy. eneuro 2017: ENEURO.0091–16.2017.

Khambhati AN, Davis KA, Lucas TH, Litt B, Bassett DS. Virtual cortical resection reveals push-pull network control preceding seizure evolution. Neuron 2016; 91: 1170–82.

Khambhati AN, Davis KA, Oommen BS, Chen SH, Lucas TH, Litt B, et al. Dynamic network drivers of seizure generation, propagation and termination in human neocortical epilepsy. PLoS Comput Biol 2015; 11: e1004608.

Kini LG, Davis KA, Wagenaar JB. Data integration: combined imaging and electrophysiology data in the cloud. Neuroimage 2016; 124: 1175–81.

Klyachko VA, Stevens CF. Connectivity optimization and the positioning of cortical areas. Proc Natl Acad Sci USA 2003; 100: 7937–41.

Ko AL, Darvas F, Poliakov A, Ojemann J, Sorensen LB. Quasi-periodic fluctuations in default mode network electrophysiology. J Neurosci 2011; 31: 11728–32.

Kopell N, Ermentrout GB, Whittington MA, Traub RD. Gamma rhythms and beta rhythms have different synchronization properties. Proc Natl Acad Sci 2000; 97: 1867–72.

Kramer MA, Cash SS. Epilepsy as a disorder of cortical network organization. Neurosci 2012; 18: 360–72.

Kramer MA, Eden UT, Kolaczyk ED, Zepeda R, Eskandar EN, Cash SS. Coalescence and fragmentation of cortical networks during focal seizures. J Neurosci 2010; 30: 10076–85.

Kwan P, Schachter SC, Brodie MJ. Drug-resistant epilepsy. N Engl J Med 2011; 10365: 919–26.

Lachaux JP, Rudrauf D, Kahane P. Intracranial EEG and human brain mapping. J Physiol Paris 2003; 97: 613–28.

Latora V, Marchiori M. Efficient behavior of small-world networks. Phys Rev Lett 2001; 87: 198701.

Latora V, Marchiori M. Economic small-world behavior in weighted networks. Eur Phys J B 2003; 32: 249–63.

Lewis JD, Theilmann RJ, Sereno MI, Townsend J. The relation between connection length and degree of connectivity in young adults: a DTI analysis. Cereb Cortex 2009; 19: 554–62.

Liang H, Wang H, Reus M de, Heuvel M van den, Berman M, McIntosh A, et al. Structure-function network mapping and its assessment via persistent homology. PLos Comput Biol 2017; 13: e1005325.

Litt B, Esteller R, Echauz J, D'Alessandro M, Shor R, Henry T, et al. Epileptic seizures may begin hours in advance of clinical onset: a report of five patients. Neuron 2001; 30: 51–64.

Liu W, An D, Tong X, Niu R, Gong Q, Zhou D. Region-specific connectivity in patients with periventricular nodular heterotopia and epilepsy: a study combining diffusion tensor imaging and functional MRI. Epilepsy Res 2017; 136: 137–42.

Logothetis NK, J P, M A, T T, A O. Neurophysiological investigation of the basis of the fMRI signal. Nature 2001: 1–8.

Lopes MA, Richardson MP, Abela E, Rummel C, Schindler K, Goodfellow M, et al. Elevated ictal brain network ictogenicity enables prediction of optimal seizure control. Front Neurol 2018; 9: 98.

Luders H, LoRusso G, Miller JP, Gonzalez-Martinez J, Kahane P, Lhatoo S. Stereotactic electroencephalography (SEEG) in the presurgical investigation of refractory focal epilepsy. Epilepsy Curr 2013; 13: 492.

Ludwig KA, Miriani RM, Langhals NB, Joseph MD, Anderson DJ, Kipke DR. Using a common average reference to improve cortical neuron recordings from microelectrode arrays. J Neurophysiol 2009; 101: 1679–89.

Mamata H, Mamata Y, Westin C-F, Shenton ME, Kikinis R, Jolesz FA, et al. High-resolution line scan diffusion tensor MR imaging of white matter fiber tract anatomy. AJNR Am J Neuroradiol 2002; 23: 67–75.

Marchi A, Giusiano B, King M, Lagarde S, Trébuchon-Dafonseca A, Bernard C, et al. Postictal electroencephalographic (EEG) suppression: a stereo-EEG study of 100 focal to bilateral tonic-clonic seizures. Epilepsia 2019; 60: 63–73.

Meroni A, Galli C, Bramerio M, Tassi L, Colombo N, Cossu M, et al. Nodular heterotopia: a neuropathological study of 24 patients undergoing surgery for drug-resistant epilepsy. Epilepsia 2009; 50: 116–24.

Micheloyannis S, Pachou E, Stam CJ, Vourkas M, Erimaki S, Tsirka V. Using graph theoretical analysis of multi channel EEG to evaluate the neural efficiency hypothesis. Neurosci Lett 2006; 402: 273–7.

Miller KJ, Leuthardt EC, Schalk G, Rao RPN, Anderson NR, Moran DW, et al. Spectral changes in cortical surface potentials during motor movement. J Neurosci 2007; 27: 2424–32.

Morris HH, Lüders H. Electrodes. Electroencephalogr Clin Neurophysiol Suppl 1985; 37: 3–26.

Mosher JC, Leahy RM. Recursive MUSIC: a framework for EEG and MEG source localization. IEEE Trans Biomed Eng 1998; 45: 1342–54.

Muldoon SF, Bridgeford EW, Bassett DS, Moreno Y, Zhou CS. Small-world propensity and weighted brain networks. Sci Rep 2016; 6: 22057.

Onnela JP, Saramäki J, Kertész J, Kaski K. Intensity and coherence of motifs in weighted complex networks. Phys Rev E - Stat Nonlinear Soft Matter Phys 2005; 71: 065103.

Otsu N. Threshold selection method from gray level histograms. IEEE Trans Syst Man Cybern 1979; SMC-9: 62–6.

Owen LLW, Manning JR. Towards human Super EEG. bioRxiv 2017: 1–20.

Park B, Eo J, Park H-J. Structural brain connectivity constrains within-a-day variability of direct functional connectivity. Front Hum Neurosci 2017; 11: 408.

Pedersen M, Omidvarnia AH, Walz JM, Jackson GD. Increased segregation of brain networks in focal epilepsy: An fMRI graph theory finding. NeuroImage Clin 2015; 8: 536–42.

Penfield W, Jasper H. Epilepsy and the functional anatomy of the human brain. JAMA J Am Med Assoc 1954; 155: 86.

Pittau F, Grova C, Moeller F, Dubeau F, Gotman J. Patterns of altered functional connectivity in mesial temporal lobe epilepsy. Epilepsia 2012; 53: 1013–23.

Plummer C, Harvey AS, Cook M. EEG source localization in focal epilepsy: where are we now? Epilepsia 2008; 49: 201–18.

Proix T, Bartolomei F, Guye M, Jirsa VK. Individual brain structure and modelling predict seizure propagation. Brain 2017; 140: 641–54.

Rafal RD, Koller K, Bultitude JH, Mullins P, Ward R, Mitchell AS, et al. Connectivity between the superior colliculus and the amygdala in humans and macaque monkeys: virtual dissection with probabilistic DTI tractography. J Neurophysiol 2015; 114: 1947–62.

Raj A, Mueller SG, Young K, Laxer KD, Weiner M. Network-level analysis of cortical thickness of the epileptic brain. Neuroimage 2010; 52: 1302–13.

Rubinov M, Sporns O. Complex network measures of brain connectivity: uses and interpretations. Neuroimage 2010; 52: 1059–69.

Rubinov M, Sporns O, van Leeuwen C, Breakspear M. Symbiotic relationship between brain structure and dynamics. BMC Neurosci 2009; 10: 55.

Rubinov M, Ypma RJF, Watson C, Bullmore ET. Wiring cost and topological participation of the mouse brain connectome. Proc Natl Acad Sci 2015; 112: 10032–7.

Salvador R, Suckling J, Coleman MR, Pickard JD, Menon D, Bullmore E. Neurophysiological architecture of functional magnetic resonance images of human brain. Cereb Cortex 2004; 15: 1332–42.

Shah P, Bassett DS, Wisse LEM, Detre JA, Stein JM, Yushkevich PA, et al. Structural and functional asymmetry of medial temporal subregions in unilateral temporal lobe epilepsy: A 7T MRI study. Human Brain Mapping 2019; 40: 2390–8.

Sinha N, Dauwels J, Kaiser M, Cash SS, Brandon Westover M, Wang Y, et al. Predicting neurosurgical outcomes in focal epilepsy patients using computational modelling. Brain 2017; 140: 319–32.

Skudlarski P, Jagannathan K, Calhoun VD, Hampson M, Skudlarska BA, Pearlson G. Measuring brain connectivity: diffusion tensor imaging validates resting state temporal correlations. Neuroimage 2008; 43: 554–61.

So NK, Blume WT. The postictal EEG. Epilepsy Behav 2010; 19: 121.

Spencer SS, Berg AT, Vickrey BG, Sperling MR, Bazil CW, Shinnar S, et al. Predicting long-term seizure outcome after resective epilepsy surgery: the Multicenter Study. Neurology 2005; 65: 912–8.

Stam CJ. Functional connectivity patterns of human magnetoencephalographic recordings: a 'small-world' network? Neurosci Lett 2004; 355: 25–8.

Taylor PN, Han CE, Schoene-Bake J-C, Weber B, Kaiser M. Structural connectivity changes in temporal lobe epilepsy: spatial features contribute more than topological measures. Neuroimage Clin 2015; 8: 322–8.

Taylor PN, Sinha N, Wang Y, Vos SB, de Tisi J, Miserocchi A, et al. The impact of epilepsy surgery on the structural connectome and its relation to outcome. NeuroImage Clin 2018; 18: 202–14.

De Tisi J, Bell GS, Peacock JL, McEvoy AW, Harkness WF, Sander JW, et al. The long-term outcome of adult epilepsy surgery, patterns of seizure remission, and relapse: a cohort study. Lancet 2011; 378: 1388–95.

Tuch DS, Reese TG, Wiegell MR, Makris N, Belliveau JW, Van Wedeen J. High angular resolution diffusion imaging reveals intravoxel white matter fiber heterogeneity. Magn Reson Med 2002; 48: 577–82.

Tzourio-Mazoyer N, Landeau B, Papathanassiou D, Crivello F, Etard O, Delcroix N, et al. Automated anatomical labeling of activations in SPM using a macroscopic anatomical parcellation of the MNI MRI single-subject brain. Neuroimage 2002; 15: 273–89.

Vaessen MJ, Jansen JFA, Vlooswijk MCG, Hofman PAM, Majoie HJM, Aldenkamp AP, et al. White matter network abnormalities are associated with cognitive decline in chronic epilepsy. Cereb Cortex 2012; 22: 2139–47.

Varotto G, Tassi L, Franceschetti S, Spreafico R, Panzica F. Epileptogenic networks of type II focal cortical dysplasia: a stereo-EEG study. Neuroimage 2012; 61: 591–8.

Vlooswijk MCG, Vaessen MJ, Jansen JFA, de Krom MCFTM, Majoie HJM, Hofman PAM, et al. Loss of network efficiency associated with cognitive decline in chronic epilepsy. Neurology 2011; 77: 938–44.

Wagenaar JB, Brinkmann BH, Ives Z, Worrell GA, Litt B. A multimodal platform for cloud-based collaborative research. In: 2013 6th International IEEE/EMBS Conference on Neural Engineering (NER). IEEE; 2013. p. 1386–1389.

Wang S, Peterson DJ, Gatenby JC, Li W, Grabowski TJ, Madhyastha TM. Evaluation of field map and nonlinear registration methods for correction of susceptibility artifacts in diffusion MRI. Front Neuroinform 2017; 11: 17.

Watts DJ, Strogatz SH. Collective dynamics of |[lsquo]|small-world|[rsquo]| networks. Nature 1998; 393: 440–2.

Wenzel M, Hamm JP, Peterka DS, Yuste R. Reliable and elastic propagation of cortical seizures in vivo. Cell Rep 2017; 19: 2681–93.

Wiebe S. Epilepsy: Outcome patterns in epilepsy surgery—the long-term view. Nat Rev Neurol 2012; 8: 123–4.

Willie JT, Laxpati NG, Drane DL, Gowda A, Appin C, Hao C, et al. Real-time magnetic resonance-guided stereotactic laser amygdalohippocampotomy for mesial temporal lobe epilepsy. Neurosurgery 2014; 74: 569–84.

Wirsich J, Perry A, Ridley B, Proix T, Golos M, Bénar C, et al. Whole-brain analytic measures of network communication reveal increased structure-function correlation in right temporal lobe epilepsy. NeuroImage Clin 2016; 11: 707–18.

World Health Organization. Epilepsy. WHO fact sheet 2018.

Yeh FC, Wedeen VJ, Tseng WYI. Generalized q-sampling imaging. IEEE Trans Med Imaging 2010; 29: 1626–35.

Zalesky A, Fornito A, Harding IH, Cocchi L, Yücel M, Pantelis C, et al. Whole-brain anatomical networks: Does the choice of nodes matter? Neuroimage 2010; 50: 970–83.

Zhang D, Snyder AZ, Shimony JS, Fox MD, Raichle ME. Noninvasive functional and structural connectivity mapping of the human thalamocortical system. Cereb Cortex 2010; 20: 1187–94.

Zhang Y, van Drongelen W, Kohrman M, He B. Three-dimensional brain current source reconstruction from intra-cranial ECoG recordings. Neuroimage 2008; 42: 683–95.

Zhang Z, Liao W, Chen H, Mantini D, Ding JR, Xu Q, et al. Altered functional-structural coupling of large-scale brain networks in idiopathic generalized epilepsy. Brain 2011; 134: 2912–28.